



ΠΑΝΕΠΙΣΤΗΜΙΟ ΚΡΗΤΗΣ - ΤΜΗΜΑ ΕΦΑΡΜΟΣΜΕΝΩΝ ΜΑΘΗΜΑΤΙΚΩΝ
Archimedes Center for Modeling, Analysis & Computation
UNIVERSITY OF CRETE - DEPARTMENT OF APPLIED MATHEMATICS
Archimedes Center for Modeling, Analysis & Computation



ACMAC's PrePrint Repository

Structure and Dynamics of Poly(methyl-methacrylate)/Graphene systems through Atomistic Molecular Dynamics Simulations

A. Rissanou and Vagelis A. Harmandaris

Original Citation:

Rissanou, A. and Harmandaris, Vagelis A.

(2013)

Structure and Dynamics of Poly(methyl-methacrylate)/Graphene systems through Atomistic Molecular Dynamics Simulations.

Journal of Nanoparticle Research.

(In Press)

This version is available at: <http://preprints.acmac.uoc.gr/175/>

Available in ACMAC's PrePrint Repository: March 2013

ACMAC's PrePrint Repository aim is to enable open access to the scholarly output of ACMAC.

<http://preprints.acmac.uoc.gr/>

Structure and Dynamics of Poly(methyl-methacrylate)/Graphene systems through Atomistic Molecular Dynamics Simulations

Anastassia N. Rissanou^{1,2*} and Vagelis Harmandaris^{1,2*}

1. Department of Applied Mathematics, University of Crete, GR-71409, Heraklion, Crete, Greece.
2. Institute of Applied and Computational Mathematics (IACM), Foundation for Research and Technology Hellas (FORTH), GR-71110 Heraklion, Crete, Greece.

Keywords: Graphene Nanocomposites – Polymer – Simulations – Structure - Dynamics

Abstract

The main goal of the present work is to examine the effect of graphene layers on the structural and dynamical properties of polymer systems. We study hybrid poly(methyl methacrylate) (PMMA)/graphene interfacial systems, through detailed atomistic molecular dynamics (MD) simulations. In order to characterize the interface, various properties related to density, structure and dynamics of polymer chains are calculated, as a function of the distance from the substrate. A series of different hybrid systems, with width ranging between $[2.60 - 13.35] \text{ nm}$, are being modeled. In addition, we compare the properties of the macromolecular chains to the properties of the corresponding bulk system at the same temperature. We observe a strong effect of graphene layers on both structure and dynamics of the PMMA chains. Furthermore the PMMA/graphene interface is characterized by different length scales, depending on the actual property we probe: Density of PMMA polymer chains is larger than the bulk value, for polymer chains close to graphene layers up to distances of about $[1.0-1.5] \text{ nm}$. Chain conformations are perturbed for distances up to about 2-3 radius of gyration from graphene. Segmental

* Author to whom correspondence should be addressed:
rissanou@tem.uoc.gr +30 2810393746 fax: +30 2810393701
vagelis@tem.uoc.gr +30 2810393735 fax: +30 2810393701

dynamics of PMMA is much slower close to the solid layers up to about $[2-3]nm$. Finally terminal-chain dynamics is slower, compared to the bulk one, up to distances of about 5-7 radius of gyration.

Introduction

Graphene, a two dimensional monolayer of graphite of macroscopic dimensions but of atomic thickness, was first isolated in 2004 (Novoselov et al. 2004) and since then it has caused a revolution in many scientific areas, due to its novel applications. The importance of this material is based on its exceptional physical properties (Rao et al. 2009) with emphasis to electronic properties (Catro-Neto et al. 2009), like its electron transport capacity and electrical conductivity. Moreover, the mechanical properties of graphene, such as the high intrinsic tensile strength and stiffness, are also of particular interest (Zhao et al. 2002; Tsoukleri et al. 2009; Frank et al. 2010). In addition, graphene exhibits high thermal conductivity, a very high specific surface area and is stable in air and transparent. All the above properties, in combination with its low cost, render graphene as a promising candidate for the reinforcement of polymer nanocomposites, taking the position of carbon nanotubes (Spitalsky et al. 2010).

Graphene polymer nanocomposites are based on the incorporation of graphene in polymer matrices in order to modify the properties of the hybrid (composite) system and to use it in various applications. Substantial role in the formation of graphene/polymer nanocomposites plays the exfoliation of graphite's layered structure and it's dispersion in a polymer matrix. An extensive review on different ways of exfoliation of graphite is given by Kim et al. (Kim et al. 2010), where advantages and disadvantages of each method are presented as well. The benefits, which have been reported for the hybrid system, are the improvement of the electrical, thermal, mechanical and gas barrier properties. Though, many of the studies on the reinforcement of graphene – polymer nanocomposites have used graphene oxide (Park et al. 2009; Dreyer et al. 2010; Ramanathan et al. 2008) rather than a single atomic layer of exfoliated graphene because of poor adhesion between graphene and polymer (Young et al. 2011). The improvement of the interfacial bonding between graphene and polymer matrices comprise the focus of

many experimental studies through various methods, like chemical bonding between graphene and polymer (Ramanathan et al. 2008; Fang et al. 2009) or the creation of a polymer crystalline layer on the graphene surface (Das et al. 2009). In this aspect Lv et al. (Lv et al. 2010) have studied, through a simulation study, the influence of the chemical functionalization of graphene on the interfacial bonding characteristics. They have used two well known polymers, polyethylene (PE) and poly(methyl methacrylate) (PMMA), as polymer matrices, and they have found that the functional groups of the graphene increase the interfacial bonding between the graphene and the polymer.

Besides experiments, simulation approaches are valuable tools for the study of molecule/graphene hybrid nanostructured systems at the molecular level. An interesting study of Awasthi et al. (Awasthi et al. 2009) focused on the graphene-polyethylene interfacial mechanical behavior using molecular dynamics (MD) simulations. They have examined the force separation behavior between graphene and polymer matrix. They have found that during the separation process a few polymer chains, the ones which are close to the graphene layer, stay adhered to it and away from the rest chains, causing voids to the polymer matrix, which gradually lead to complete separation, i.e. cohesive failure of the hybrid materials has been observed.

Another interesting aspect of graphene-polymer composites is the way that graphene layers affect the properties of polymers, compared to their bulk behavior. This question belongs to the area of polymer-interface problems (Fleer et al 1993; Jones et al. 1999). Although there is a large amount of both experimental (Zheng et al. 1997; Frank et al. 1996; Lin et al. 1997; Rivillon et al. 2000; Anastasiadis et al. 2000; Fotiadou et al. 2010; Chrissopoulou et al. 2011) and simulation studies (Mansfield et al. 1989 and 1991; Bitsanis et al. 1990; Rissanou et al. 2009; Karaiskos et al. 2009) on the general topic of polymer/solid interfaces, here we focus more on polymer/graphene (or polymer/graphite) simulation works, which are more relevant to our work. In more detail, Harmandaris et al. and Daoulas et al. (Daoulas et al. 2005), in a series of two papers reported on modeling of hybrid polymer/graphite systems, through state-of-the-art atomistic Monte Carlo and Molecular Dynamics (MD) simulations. The influence of the graphite surface on the structure, conformations and dynamics of the polymer chains was studied in the atomic level. Recently in another simulation work (Yang et al. 2011) the crystallization

process of alkane melts on carbon nanotubes (CNT) and graphene nanosheets (GNS) has been studied. For a series of different polymers authors found that both CNTs and GNSs induce crystallization of alkane molecules in the range of temperatures $[400-500]K$, while CNT's presented a stronger effect on crystallization. The structure of atactic polystyrene (PS) on three different substrates, α -quartz, amorphous silica and graphite has been also studied through detailed atomistic simulations by Tatek et al. (Tatek et al. 2011). In this work the effect of the type of the different surfaces on the density, the structure and the conformational properties of PS has been discussed.

Here we examine the conformations and the properties of the polymer chains of a hybrid system which is comprised by PMMA and graphene, using atomistic molecular dynamics simulations. The structural and dynamical properties of atactic PMMA chains as a function of distance from the graphene surface are examined. The results are compared with the corresponding bulk system. Our model represents a number of graphene layers dispersed in a polymer matrix, as it is explained with more details in the corresponding section; the current study also exhibits the effect of confinement of a polymer film between two graphene layers as a function of the thickness of the film.

The present work is the first part of a general computational approach for the study of realistic polymer/graphene systems, with main goal the prediction of the macroscopic properties of realistic nanocomposites and their dependence on the structural characteristics at the atomic level, especially at the interface. To succeed this, a hierarchical multi scale methodology (Harmandaris et al. 2009; Harmandaris et al. 2010) is necessary, which involves density functional theory (DFT), classical molecular dynamics (MD) as well as mesoscopic coarse-grained dynamics simulations (Johnson et al. 2011). The overall methodology will allow us to provide a fundamental study of the coupling between microstructure at the interface and macroscopic properties (structural, mechanical, elastic and dynamical-rheological) of graphene/polymer nanocomposite systems.

The paper is organized as follows: The second section contains a description of the simulation method, our model and the details for the simulated systems. Our results are presented in the third section, where a division in structural, conformational and

dynamical properties has been made. Finally, a summary and the conclusions of the current study are presented.

Simulation Method and Systems

Atomistic *NPT* and *NVT* Molecular Dynamics (MD) simulations of model PMMA/graphene systems were performed using the GROMACS code (Berendsen et al. 1995; Lindahl et al. 2001; Hess et al. 2008). For *NPT* simulations the pressure was kept constant at $P=1atm$, using a Berendsen barostat. The stochastic velocity rescaling thermostat (Bussi et al. 2007) was used to maintain the temperature value at $T=500K$. An all atom representation model has been used for both PMMA and graphene. The atomistic force field, which has been used for the description of the intermolecular and intramolecular interactions of PMMA, is based on OPLS (Jorgensen et al. 1996; Price et al. 2001). For the interaction between polymer atoms and graphene layers the geometric means $\epsilon_{ij} = (\epsilon_{ii}\epsilon_{jj})^{0.5}$ and $\sigma_{ij} = (\sigma_{ii}\sigma_{jj})^{0.5}$ were calculated with: $\epsilon_{cc}/k_B=28K$ and $\sigma_{cc}=3.4\text{\AA}$ (Steele 1973). Graphene has been represented as a set of LJ carbon atoms, centered at their crystallographic positions. We have used an in-plane lattice constant of graphite of about 2.462\AA . This value has been obtained from experimental data at $300K$, and it is independent of temperature for a very broad range of temperatures (Pozzo et al. 2011). At this point, no interactions were assumed between graphene atoms, which remained fixed in space during the simulation. Table 1 contains all the energetic parameters which have been used in our simulations and atom types are defined on the snapshot of PMMA monomer, which is lying in the last column of table 1.

Bond lengths were constrained by means of ‘LINCS’ (Linear Constraint Solver), algorithm (Hess et al. 1997). The time step was $0.001ps$ and a cutoff distance of 10\AA for the non bonded interaction was used. Periodic boundary conditions have been used in all three directions, so that the polymer interacts with the graphene layer, which was placed at the bottom of the simulation box, on the xy plane and its periodic image at the top of the simulation box simultaneously. This setup renders our system a polymer film confined between two graphene surfaces. Moreover, interaction exists between the

polymer in the simulation box and its periodic images. Therefore, the overall model description refers to a system of graphene layers dispersed in a polymer matrix. We should note here that the latter refers to ideal dispersion, which is certainly not the usual case for realistic nanocomposites (Koo 2006). However we do not expect this assumption model to introduce artifacts in the polymer behavior since we are particular interested in large (compared to chain size) graphene layers and short time dynamics, i.e. the motion of the layers is not important. Furthermore, the model systems are much larger than chain dimensions, both in x and y direction, showing no system size effects.

Equilibration of polymer chains is in general a non-trivial issue. In our study, in order to equilibrate the systems, we first performed MD simulations at high temperature (i.e., $800K$) until decorrelation of the end-to-end vector was succeeded. Then, annealing up to $500K$ with various cooling rates was performed in order to check the effect of the cooling rate on the properties of the final system. Here we report data using a cooling rate of $2K/ns$. Afterwards, NPT simulations of $100ns$ were performed in order to attain a ‘constant’ density value. Finally, statistics was gathered from the production runs, which were performed in the NVT statistical ensemble for another $0.5\mu s$. For the simulations we have used a 12-core machine CPUs Intel(R) Xeon(R) CPU X5650 @ $2.67GHz$. A typical simulation run of $100ns$, for the largest model system, takes about 8 days in such a machine.

Setup details for the simulated systems are depicted in Table 2, where N is the number of polymer chains in the simulation box. In all cases we model all-atom atactic PMMA 10-mers. In order to compare with bulk behavior we have also modeled a reference bulk system that consists of 54 10-mer PMMA chains. For the bulk system we have first performed NPT simulations at $T=500K$, and the average density of the NPT runs was $1.054g/cm^3$, for the model system studied here. Then NVT simulation was performed at the above density, in order to do equivalent comparisons with the confined systems. The experimental value for the density of atactic PMMA at $500K$ has been reported equal to $1.067g/cm^3$ (Wunderlich 1989) and is slightly underestimated by our model. Tests for higher molecular lengths have been performed and do not alter the results. The film thickness (d), which is included in the third column of Table 2, is calculated from the box length along the z -direction subtracting the thickness of the

graphene layer, 0.34nm (i.e of the order of one van der Waals radius), which is placed at $z=0$. The mass fraction of the graphene (mass of graphene / total mass of the system) in the model composite is quite large in all systems (from 10% - 37%) and is depicted in the fourth column of Table 2.

Results and Discussion

First, in Figure 1a we present a snapshot from an equilibrated conformation of a confined PMMA film between two graphene layers, separated by a distance of 2.94nm , which contains 27 PMMA chains. In Figure 1b we show the all atom representations of a model PMMA dimer.

Structural Properties

We start the discussion of simulation results with the presentation of structural properties of graphene-polymer nanocomposites.

Density profiles of polymer films, with respect to z -axis, reflect the attraction of polymers from the graphene surface. Figure 2 presents the density profile for all PMMA systems as a function of distance from graphene layers (r). Density profiles are based on the monomer center of mass and are averaged over time. Their definition is the ratio of the mass of the monomers, whose center of mass lies in a specific distance from the graphene layer, over the volume of the simulation box. Systems PMMA1 and PMMA2 are depicted in Figure 2a while the rest three systems (PMMA3, PMMA4 and PMMA5) are depicted in Figure 2b. A common observation for all systems is that density profiles are symmetrical with respect to the center of the film, though small differences are observed in the curves' features between the two surfaces, due to statistical uncertainties. The high peak near the graphene surface denotes the attraction of PMMA from the graphene layer. Bulk density, which is represented by a horizontal dashed line, is attained in the middle of the polymer films, for all systems, except for the very confined one (PMMA1), for which the density profile is noisier.

A more detailed picture for the polymer's arrangement with respect to the surface is provided by the density profiles of individual groups of atoms, which are depicted in

Figure 3 and Figure 4. First, we analyze the density distributions based on end and inner parts of the polymer chain. The end part contains two monomers, the first and the last one, while the inner part is defined as the part of the chain which is contained in the interval $\left[\left(\frac{N}{2} - 2\right) - \left(\frac{N}{2} + 2\right)\right]$. Results for the biggest system (PMMA5) are depicted in

Figure 3. We observe that end monomers prefer to stand close to the surface in contrast to the inner part of the chain which is distributed homogeneously in between the two surfaces. Qualitatively similar results have been reported for other systems in the literature, like polyethylene/graphite interfaces (Daoulas et al 2005).

Second, polymer chains are analyzed in the level of backbone and side groups as it is presented in Figure 4. PMMA has two kinds of side groups, the methyl and the carboxyl group. Density values have been normalized with the corresponding bulk density. Figures 4a and 4b present results for two systems the smallest and the biggest one respectively. For the biggest system data have been symmetrized along z-axis and are presented up to the center of the polymer film. The attraction between graphene layers and PMMA chains is equivalent for backbone and side groups for the biggest system, where the most structureless density curve is the one that corresponds to carboxyl group. On the contrary, for the thinnest PMMA film (PMMA1 system) the effect of confinement becomes very important: We observe that the maximum in the distribution of the backbone of the chain has been slightly moved further away from the surface. In addition the distribution of PMMA side groups shows structure in more than one layer. In practice, this system has been trapped in a metastable state, with a specific polymer arrangement and remains almost frozen, away from equilibrium, as it will be also discussed later. Finally, it would have been interesting to compare PMMA density profiles, obtained from the simulations, with experimental data. However, we are not aware of any experimental study of density of PMMA/graphene systems, for such short chains.

Polymer Conformations

In the next stage we analyze the polymer dimensions and conformations for the various model systems studied here. Information for the conformational properties of the polymer

chain, on the segmental level, can be obtained through the calculation of the second rank bond order parameter, $P_2(\cos\theta)$ (Kotelyanskii et al. 2004; Turzi 2011). This order parameter provides detailed information for the orientation of individual parts of the polymer chain and is given by:

$$P_2(\cos\theta) = \frac{3}{2} \langle \cos^2 \theta \rangle - \frac{1}{2}$$

where, θ is the angle between an arbitrary vector, which is defined along the molecule, and one Cartesian axis. Here we are using the z -axis, which is normal to the surface, in order to characterize chain structure as a function of distance from the graphene layers. We have defined two characteristic vectors on PMMA molecule, which have been drawn on the dimer of Figure 1b. The first vector, denoted by \mathbf{v}^{bb} , has been defined along the molecule's backbone, while the second one, \mathbf{v}^{bc} , is defined from the backbone's carbon, to the carboxyl oxygen. Note that a value of -0.5 for $P_2(\cos\theta)$ denotes a vector with orientation parallel to surface, a value of 1.0 normal to the surface, and a value of 0.0 random orientation with respect to the surface.

In order to examine the effect of the surface on the orientational order at the monomeric level, $P_2(\cos\theta)$ was analyzed as a function of the distance from the surface. For each polymer film one adsorption layer is defined from the first minimum of the corresponding density profile, whereas a bulk region follows, which is divided into equal spaced layers of the order of $1nm$. In Figures 5a and 5b we present the bond order parameter $P_2(\cos\theta)$ along z -axis, for two systems. Trying to avoid the effects of the strong confinement (i.e, trapping in metastable states) we chose the third (Figure 5a) and the fifth (Figure 5b) system. We have averaged data over the equal distances from the two graphene layers in order to improve statistics, utilizing system's symmetry. Thus, the data for the z component of the bond order parameter $P_2(\cos\theta)$, as a function of distance from graphene, start from the origin (i.e., position of the graphene layer) and end to the middle of the simulation box. Dashed normal lines in Figures 5a and 5b indicate the area of the first adsorption layer. In this layer, which is up to $0.5nm$ from the graphene surface, $P_2(\cos\theta)$ values of \mathbf{v}^{bb} for both PMMA3 and PMMA5 are negative, in the range of $[(-0.3) - (-0.2)]$, which indicates that backbone tends to an almost parallel to the surface orientation ($P_2 = -0.5$ corresponds to $\theta = 90^\circ$). At longer distances $P_2(\cos\theta)$ has values

close to zero and consequently suggests a random orientation. In addition, \mathbf{v}^{bc} attains higher values close to the surface $\sim (-0.15)$, which indicates a smaller tendency of the side group to be oriented parallel to the graphene layer. This can be attributed to the fact that side group has higher flexibility, which randomizes its orientation easier, compared to the backbone.

The mean size of the entire polymer chain is quantified by both average radius of gyration, $\langle R_g \rangle$ and end-to-end distance $\langle R_{ee} \rangle$ which are included in Table 2. The values for bulk PMMA are also included. Comparisons of both R_g and R_{ee} values among all polymer films and the bulk system indicate that the size of the polymer chain is almost equal to the respective bulk value for all film thicknesses except for the thinner films, which are trapped in metastable non-equilibrium conditions.

Supplementary conformational analysis, on the entire chain level, can be obtained from the calculation of the conformation tensor. Conformation tensor is defined as the second moment of the end-to-end distance through:

$$C_{\alpha\beta} = 3 \left\langle \frac{R_{ee\alpha} R_{ee\beta}}{\langle R_{ee}^2 \rangle_0} \right\rangle$$

where, $\langle R_{ee}^2 \rangle_0$ is the mean end-to-end distance of an unperturbed chain (i.e. bulk polymer system) and α, β are the x, y, z components. This tensor describes the entire chain's conformations and its deviation from the equilibrium value $\mathbf{C}=\mathbf{I}$ (i.e., unit tensor) provide information for the orientation and the extension of the chain.

Here, conformation tensor components, $C_{\alpha\beta}$, have been calculated as a function of the distance from the surface, based on the layers discretization described above. In more detail, we present results for the components which are perpendicular to the surface, C_{zz} , as well as parallel (in-plane) to the surface, $C_{//}$. The parallel components have been calculated as the mean value of the two in-plane components (in x and y directions), i.e. $C_{//} = (C_{xx} + C_{yy}) / 2$. The values for the conformation tensor are ensemble averages over all polymer chains, whose center of mass lie in the specific layer. Moreover data have been symmetrized along the z -axis.

In Figures 6a and 6b we present data for C_{zz} and $C_{//}$ of PMMA chains, as a function of distance from the graphene layers, for all hybrid PMMA/graphene systems studied here. Error bars are ranged between $[0.05-0.1]$ for all cases. At distances close to the graphene layer, PMMA attains conformations elongated in the xy direction and compressed in the z direction, as it is realized from the values of C_{zz} (Figure 6a) and $C_{//}$ (Figure 6b), which are lower and higher than 1.0 respectively. In addition all films show similar, within the statistical error, values for both C_{zz} and $C_{//}$. Finally, the PMMA conformations tend to the behavior of bulk PMMA beyond a distance of about 1.0-1.5nm from the graphene layers. This length scale corresponds to about 2-2.5 times the average bulk radius of gyration, R_g .

Finally, we should note here that an important point in polymer/solid interfacial systems is the analysis of polymer chain conformations in trains, tails and loops. This is a problem studied a lot in the past through theory (Fleer et al. 1993), generic bead spring coarse-grained models (Bitsanis et al.1990; Källrot et al.2007; Chremos et al. 2009), as well as atomistic simulations of simple polyethylene/graphite systems (Daoulas et al. 2005). The model PMMA chains studied here are rather short and such an analysis is not reliable. Analysis of longer PMMA chains will be the subject of a future work, which will involve systematic coarse-grained models for the representation of the polymer chains.

Dynamical Properties

In the next stage we study the dynamics of the hybrid nanocomposite systems. Dynamics of polymer chains at both segmental and molecular level is examined. Information for the mobility in the segmental-monomer level can be extracted through the calculation of time correlation functions of specific vectors. Here we are using the characteristic vectors, which have been described previously and presented in Figure 1b (\mathbf{v}^{bb} , \mathbf{v}^{bc}). In more detail we calculate the second-order bond order parameter as a function of time, through:

$$P_2(t) = \frac{3}{2} \langle \cos^2 \theta(t) \rangle - \frac{1}{2}$$

In this formula, $\theta(t)$ is the angle of the vector under consideration at time t relative to its position at $t=0$. First, we examine the average dynamics over the entire film. In Figure 7 the time autocorrelation functions of both characteristic vectors for the biggest system (PMMA5) are depicted, together with the corresponding autocorrelation functions of the bulk system. The comparison of the backbone's characteristic vector (\mathbf{v}^{bb}) with the characteristic vector of the side group (\mathbf{v}^{bc}) indicates a slower relaxation of backbone. This is an expected behavior because the motion of the side group is less constrained than the backbone's motion. Moreover, the comparison of the above vectors with the corresponding vectors of bulk system indicates that bulk's relaxation is faster. This observation renders confinement a reason of polymer's retardation. Nevertheless, we have to note that the largest film, with a thickness of about $20R_g$, exhibit segmental dynamics very close to the bulk one, as expected.

Furthermore, orientational dynamics in the entire chain level (terminal-chain dynamics) can be studied by calculating the end-to-end vector autocorrelation function defined as:

$$u(t) = \frac{\langle R_{ee}(t)R_{ee}(0) \rangle}{\langle R_{ee}^2 \rangle_0},$$

where $R_{ee}(t)$ and $R_{ee}(0)$ are the positions of the end-to-end distance at time t and 0 respectively, and $\langle R_{ee}^2 \rangle_0$ is the mean squared value of the equilibrium (unperturbed) end-to-end distance. Figure 8 contains the average time autocorrelation function of the end – to – end vector for all five systems studied here. This figure provides an estimation of the degree that confinement hinders polymer dynamics in molecular level. The effect of confinement becomes more pronounced in the whole chain level: the $u(t)$ autocorrelation function for the most confined system (PMMA1) does not decay more than 0.95 even after $0.5\mu s$, showing that this system is practically frozen for the time scale considered here. As the polymer film becomes thicker end-to-end vector decorrelates much faster.

A quantification of these differences in relaxation times is presented in Table 3. We fit the bond order parameter, $P_2(t)$, for the two characteristic vectors and the end-to-end vector autocorrelation function, $u(t)$, with stretch exponential functions (Kohlrausch-Williams-Watts, (KWW)) (Williams et al. 1970) of the form:

$$P_2(t) = A \exp \left[- \left(\frac{t}{\tau_{KWW}} \right)^\beta \right],$$

where A is a pre-exponential factor which takes into account relaxation processes at very short times (i.e., bond vibrations and angle librations), τ_{KWW} is the relaxation time and β is the stretch exponent, which takes into account the deviation from the ideal Debye behavior (Mansfield et al. 1989).

In Table 3 we present results for the five PMMA systems and for the corresponding bulk system based on the average dynamics over the entire film. The error bars for the stretching exponents β are about $[0.02-0.05]$ and for the relaxation times, τ_{KWW} , are around 10% of the actual value, for all cases. We observe that for all three vectors (\mathbf{v}^{bb} , \mathbf{v}^{bc} , R_{ee}) there is an increase in β exponent with the film thickness which indicates that the distribution of relaxation times becomes narrower as the polymer film becomes thicker (i.e. from the most to the less confined system). Moreover, for all systems, the values of β exponent are higher for the backbone's vector (\mathbf{v}^{bb}) compared to the side group's vector (\mathbf{v}^{bc}), which indicates broader distribution of relaxation times for the side group, whereas β -values for R_{ee} are even higher, at least for the last system. Comparing relaxation times we observe a decrease in their values with the film thickness for all vectors. Relaxation times for \mathbf{v}^{bb} are higher than the ones for \mathbf{v}^{bc} , which shows the faster relaxation of the side group's vector compared to the backbone's vector, as it was also mentioned above. These values are extremely large for the most confined polymer films indicating strong slowdown of the dynamics for these systems. Note also that despite the rather long atomistic MD simulations performed here (0.5 μ s), it is not possible to get reliable data about the maximum relaxation time of the entire chain, for all but the thicker film (PMMA5 system), due to very strong effect of the graphene layers on the mobility of the PMMA chains; i.e. their dynamics becomes extremely slow. Besides, the biggest system's values for both β and τ_{KWW} are the closer to the corresponding bulk values.

The effect of the graphene on the polymer dynamics is examined in more detail through the calculation of $P_2(t)$ at different distances from graphene. In Figure 9 the autocorrelation function of \mathbf{v}^{bb} for PMMA5 is presented, at different distances from the surface, as it was discussed in the previous section (i.e., one adsorption layer and

uniformly divided bulk region). The arrow's direction denotes the increasing distance from graphene. Fittings of all curves with the stretch exponential functions KWW provide values for relaxation times τ_{KWW} and exponents β . An alternative way to present relaxation times is through the definition of the segmental relaxation time, which is measured in dielectric experiments as well, and is defined as the integral of the KWW

curves through: $\tau_{segm.} = \frac{\tau_{KWW}}{\beta} \Gamma\left(\frac{1}{\beta}\right) \cdot \tau_{segm.}$ and β , as a function of distance from the

graphene layer for both \mathbf{v}^{bb} and \mathbf{v}^{bc} of PMMA5, are presented in Figures 10a and 10b respectively. Segmental relaxation times for both vectors, decreases with the distance from graphene, while beyond a certain distance, of about 3-4nm, they reach a plateau value. Moreover, for distances shorter than 2nm relaxation times are much larger (about 4 orders of magnitude for \mathbf{v}^{bb} and 2 for \mathbf{v}^{bc}) than their corresponding bulk values, which indicate the strong effect of the graphene on the mobility of PMMA segments near to the interface. In addition, relaxation times for \mathbf{v}^{bc} are smaller than the ones for \mathbf{v}^{bb} at any distance from the surface, as expected due to the higher mobility of the side groups in PMMA.

Stretch exponent's β values, for both vectors are shown in Figure 10b. It is clear that both backbone and side group segments close to graphene have smaller β values than the bulk values, i.e. their distribution of relaxation times is broader than the bulk ones. In addition, close to the surface β values are almost the same for \mathbf{v}^{bb} and \mathbf{v}^{bc} , while at longer distances, β values are slightly larger for the former vector. Beyond 2nm, β attains values in the range of [0.5-0.55] for \mathbf{v}^{bb} and in the range of [0.45-0.5] for \mathbf{v}^{bc} . These can be thought as constant values, in the range of the statistical error and are in accordance with the ones which are valid for the bulk system respectively.

Complementary information for polymer dynamics, in segmental level, can be extracted directly from the MD simulations by computing the mean square displacement (MSD) as a function of time ($\langle (R(t) - R(0))^2 \rangle$, R is the position of the chain's center of mass), which is depicted in Figure 11. Diffusion proceeds through different adsorption layers in an increasing rate, starting form very close to the graphene layer and moving towards the middle of the polymer film. Figure 11 contains the MSDs components in the

xy direction for PMMA5, as a function of time, in the two limiting cases, the closest to the graphene surface adsorption layer and the most distant one. MSD's calculations are based on the monomer center of mass. A first observation is that the closest to the surface layer has significantly slower dynamics than the faraway one. Moreover, at the closest adsorption layer a plateau is observed between [10-100] ps, which is indicative of glass transition like behavior. This is an initial sign that strong confinement affects the glass transition temperature of polymers, moving it to higher values. That will be the subject of a future work. On the contrary, as expected, there is no any plateau in bulk's mean square displacement curve. In addition, the curve, which corresponds to bulk's MSD, is close to the distant layer's MSD curve, though higher.

Finally, the mobility of the polymer in the molecular level can be described from an effective time dependent self-diffusion coefficient, given by the following formula:

$$D(t) = \frac{\langle (R(t) - R(0))^2 \rangle}{6t}. \quad D(t) \text{ describes the translational motion and its calculation is}$$

based on the center of mass of the polymer chain (R is the position of the chain's center of mass). For a homogeneous molecular system, exhibiting linear diffusion, $D(t)$ reaches a constant time independent value (self-diffusion coefficient), for times longer than about the maximum relaxation time of the molecule (polymer chain here). Figure 12 presents diffusion coefficients as a function of time for the smallest and the biggest system together with the corresponding bulk curve. For the biggest system (i.e., PMMA5) the time dependent behavior of $D(t)$ at long times tends to a plateau value after around 100ns. Furthermore, this curve almost coincides with bulk's $D(t)$. All the rest PMMA/graphene systems (PMMA4, PMMA3 and PMMA2, not shown here) exhibit much slower dynamics, being not possible to find a linear time independent regime for $D(t)$. This is particular clear for the smallest system (i.e., PMMA1), for which the continuous decrease of $D(t)$ indicates an extremely slow diffusion, which is a result of the strong confinement; (i.e. the system is practically frozen). Note that $D(t)$ should also strongly depend on the molecular length. Therefore, if we consider that the distance of the middle of the largest (PMMA5) system to graphene layers correspond to about 5-7 radius of gyration, then this is approximately the length scale up to which a strong effect of the graphene layers on the dynamics of the PMMA chains is observed.

Discussion and Conclusions

This work is the first part of a bigger project, which aims to the prediction of the macroscopic properties of graphene/polymer nanocomposites starting from molecular principles. Atomistic molecular dynamics simulations have been performed on a hybrid nanostructured system of dispersed graphene layers in a poly(methyl-methacrylate), PMMA, matrix. The effect of the graphene layers on the structural and dynamical properties of polymer systems was studied through the simulation of a series of PMMA films with different film thickness ranged from $[2.60 - 13.35]$ nm, that corresponds to a range of $4-20R_g$ (or about $2-8R_{ee}$) for the specific PMMA chains.

Density profiles, based on the monomer center of mass, indicate the attraction of PMMA from graphene surface. In addition, end monomers were found to be closer to the graphene layer compared to the inner part of the chain, as it has been reported in the literature (Daoulas et al. 2005) for other atomistic or coarse-grained (Bitsanis et al. 1990) interfacial systems. Nevertheless, there is not any difference in the strength of the attraction between the graphene layer and the backbone or the side groups (i.e. methyl and carboxyl side group) of PMMA, except for the strongly confined PMMA system. The calculation of the second rank order parameter $P_2(\cos\theta)$ revealed information for the preferable orientation of the backbone and carboxyl side group of polymer chains with respect to the surface. In both cases a parallel to the surface orientation is more favorable, although this is less pronounced for the carboxyl group of PMMA. All systems attain bulk density in the intermediate region between graphene layers, except for the very confined one, where the density profile is much noisier. Furthermore, the calculation of the conformation tensor showed that all systems tend to bulk behavior beyond distances which correspond to 2-3 times the average bulk radius of gyration.

From the point of view of dynamics, in monomer level, the backbone vector (\mathbf{v}^{bb}) was found to be slower than side group vector (\mathbf{v}^{bc}) due to the fact that side group's motion is less constrained than backbone's motion. The effect of graphene on polymer's dynamics was quantified through the calculation of the second order parameter $P_2(t)$ at

different adsorption layers. The values for the segmental relaxation times ($\tau_{segm.}$), which have been extracted from the fitting of the autocorrelation functions of the specific vectors (\mathbf{v}^{bb} and \mathbf{v}^{bc}) with the stretch exponential function KWW, show a decrease with the distance from the graphene layer. Finally, a crucial observation is that segmental dynamics ($\tau_{segm.}$) close to the surface is much slower (from 2 up to 4 orders of magnitude) than the bulk one. Therefore it is not surprised that the strongly confined systems (i.e. $d \sim R_g$), in which all PMMA atoms are very close to the graphene layers, are practically frozen, trapped in a metastable condition.

Summarizing, the length of the interfacial region in hybrid polymer/solid systems is a crucial parameter in the design of nanostructured materials with specific properties. Our detailed atomistic molecular simulations performed here, indicate clearly that the length of the interface depends crucially on the actual property we are checking: (a) Density polymer profile is different than the homogenous bulk one for polymer chains close to graphene layers up to distances of about [1.0-1.5]nm. (b) If the degree of perturbation of chain conformations is used, then the length of the interfacial region depends on the molecular length of the polymer chains, being about 2-3 radius of gyration. (c) Segmental dynamics of polymer is much slower close to the solid layers up to about [2-3]nm. (d) Finally terminal-chain dynamics is slower, compared to the bulk one, up to distances of about 5-7 radius of gyration.

Current work is along two directions. The first concerns direct detailed atomistic study of different polymer/graphene (such as polystyrene/graphene and polyethylene/graphene) systems, in order to further examine the coupling between the monomeric structure and the graphene layers at the atomic level, with particular emphasis on the dynamics (friction coefficient) of the polymer chains (*Rissanou and Harmandaris to be submitted*). The second direction, concerns the implementation of coarse-grained models in order to study larger more realistic nanostructured graphene based polymer (PMMA) nanocomposites.

Acknowledgments

The authors would like to thank Costas Galiotis, Spiros Anastasiadis, as well as, Kostas Papagelis, Giorgos Kalosakas, George Konstantinidis and George Deligeorgis for valuable discussions. Funding was provided by the Graphene Research Center. Partially supported by the European Union's Seventh Framework Programme (FP7-REGPOT-2009-1) project "Archimedes Center for Modeling, Analysis and Computation" under grant agreement 245749.

References

- Anastasiadis SH, Karatasos K, Vlachos G, Manias E, Giannelis EP (2000) Nanoscopic-Confinement Effects on Local Dynamics. *Phys. Rev. Lett.* 84:915-918.
- Awasthi AP, Lagoudas DC, Hammerand DC (2009) Modeling of graphene-polymer interfacial mechanical behavior using molecular dynamics. *Modelling Simul. Mater. Sci. Eng.* 17:015002-1 – 37.
- Berendsen H, van der Spoel D, van Drunen R (1995) GROMACS: A message-passing parallel molecular dynamics implementation. *Comp. Phys. Comm.* 91:43-56.
- Bitsanis IA, Hatzioannou G (1990) Molecular dynamics simulations of the structure and dynamics of confined polymer melts *J. Chem. Phys.* 92: 3827-3847.
- Bussi G, Donadio D, Parinello M (2007) Canonical sampling through velocity rescaling. *J. Chem. Phys.* 126:014101-1 - 014101-7.
- Catro-Neto AH, Guinea F, Peres NMR, Novoselov KS, Geim AK (2009) The Electronic Properties of Graphene. *Reviews of Modern Physics* 81(1):109-155.
- Chremos A, Glynos E, Koutsos V, Camp PJ (2009) Adsorption and self-assembly of linear polymers on surfaces: a computer simulation study. *Soft Matter* 5: 637-645.
- Chrissopoulou K, Andrikopoulos KS, Fotiadou S, Bolas S, Karageorgaki C, Christofilos D, Voyiatzis GA, Anastasiadis SH (2011) Crystallinity and Chain Conformation in PEO/Layered Silicate Nanocomposites. *Macromolecules* 44:9710-9722.

- Daoulas KC, Harmandaris VA, Mavrantzas VG (2005) Detailed Atomistic Simulation of a Polymer Melt/Solid Interface: Structure, Density and Conformation of a Thin Film of Polyethylene Melt Adsorbed on Graphite. *Macromolecules* 38:5780-5795; (2005) Molecular Dynamics Simulation of a Polymer Melt/Solid Interface: Local Dynamics and Chain Mobility in a Thin Film of Polyethylene Melt Adsorbed on Graphite. *Macromolecules* 38:5796-5809.
- Das B, Prasad KE, Ramamutry U, Rao CNR (2009) Nano-indentation studies on polymer matrix composites reinforced by few-layer graphene. *Nanotechnology* 20(12):125705-125709.
- Dreyer DR, Park SJ, Bielawski CW, Ruoff RS (2010) The chemistry of Graphene Oxide. *Chem. Soc. Rev.* 39:228-240.
- Fang M, Wang KG, Lu HB, Yang YL, Nutt S (2009) Covalent polymer functionalization of graphene nanosheets and mechanical properties of composites. *J. Mater. Chem* 19(38):7098-7105.
- Fleer GJ, Cohen Stuart MA, Scheutjens JM, Cosgrove T, Vincent B (1993) *Polymers at Interfaces*. Chapman & Hall: London.
- Fotiadou S, Chrissopoulou K, Frick B, Anastasiadis SH (2010) Structure and dynamics of polymer chains in hydrophilic nanocomposites. *J Pol Sci. Part B Pol. Phys* 48:1658-1667.
- Frank B, Cast AP, Russel TP, Brown HR, Hawker C (1996) Polymer Mobility in Thin Films. *Macromolecules* 29:6531-6534.
- Frank O, Tsoukleri G, Parthenios J, Papagelis K, Riaz I, Jalil R, Novoselov KS, Galiotis C (2010) Compression Behavior of Single-Layer Graphenes. *ACS NANO* 4(6):3131-3138.
- Harmandaris V, Kremer K (2009) Dynamics of polystyrene melts through hierarchical multiscale simulations. *Macromolecules* 42:791-802; (2009) Predicting polymer dynamics at multiple length and time scales. *Soft Matter* 5:3920-3926.
- Harmandaris V, Baig C (2010) Quantitative Analysis on the Validity of a Coarse-Grained Model for Nonequilibrium Polymeric Liquids under Flow. *Macromolecules* 43:3156-3160.

- Hess B, Bekker H, Berendsen HJC, Fraaije JGEM (1997) LINCS: A linear constraint solver for molecular simulations. *J. Comp. Chem.* 18: 1463-1472.
- Hess B, Kutzner C, van der Spoel D, Lindahl E (2008) GROMACS 4: Algorithms for highly efficient, load-balanced, and scalable molecular simulation. *Journal of Chemical Theory and Computation*, 4:435-447.
- Johnson K, Harmandaris V (2011) Properties of Benzene Confined between Two Au(111) Surfaces Using a Combined Density Functional Theory and Classical Molecular Dynamics Approach. *J. Phys. Chem. C* 115:14707-14717; (2012) Properties of short polystyrene chains confined between two gold surfaces through a combined density functional theory and classical molecular dynamics approach. *Soft Matter* 8:6320-6332.
- Jones RAL, Richards RW (1999) *Polymers at surfaces and Interface*. Cambridge University Press: Cambridge.
- Jorgensen WL, Maxwell DS, Tirado-Rives J (1996) Development and Testing of the OPLS All-Atom Force Field on Conformational Energetics and Properties of Organic Liquids. *J. Am. Chem. Soc.* 118:11225-11236.
- Källrot N, Linse P (2007) Dynamic Study of Single-Chain Adsorption and Desorption. *Macromolecules* 40: 4669-4679.
- Karaiskos E, Bitsanis IA, Anastasiadis SH (2009) Monte Carlo studies of tethered Chains. *J. Pol. Sci. Part B: Pol. Phys.* 47:2449-2461.
- Kim H, Abdala AA, Macosko CW (2010) Graphene/Polymer Nanocomposites. *Macromolecules* 43:6515-6530.
- Koo J (2006) *Polymer Nanocomposites: Processing, Characterization, And Applications*, McGraw-Hill.
- Kotelyanskii M, Theodorou DN (2004) *Simulation Methods for Polymers*. Marcel Dekker Inc. New York - Basel.
- Lin E, Wu W, Satija S (1997) Polymer Interdiffusion near an Attractive Solid Substrate. *Macromolecules* 30:7224-7231.
- Lindahl E, Hess B, van der Spoel D (2001) GROMACS 3.0: A package for molecular simulation and trajectory analysis. *J. Mol. Model.* 7:306-317.

- Lv C, Xue Q, Xia D, Ma M, Xie J, Chen H (2010) Effect of Chemisorption on the Interfacial Bonding Characteristics of Graphene-Polymer Composites. *J Phys Chem* 114:6588-6594.
- Mansfield KF, Theodorou DN (1989) Interfacial structure and dynamics of macromolecular liquids: a Monte Carlo simulation approach. *Macromolecules* 22:3143-3152; (1991) Atomistic simulation of a glassy polymer/graphite interface. 24 4295-4309.
- Novoselov KS, Geim AK, Morozov SV, Jing D, Zhang Y, Dubonos SV, Grigorieva IV, Firsov AA (2004) Electric Field Effect in Atomically Thin Carbon Films. *Science* 306(5696):666-669.
- Park SJ, Ruoff RS (2009) Chemical Methods for the Production of Graphenes. *Nat. Nanotechnol.* 4:217-224.
- Pozzo M, Alfè D, Lacovig P, Hofmann P, Lizzit S, Baraldi A (2011) Thermal Expansion of Supported and Freestanding Graphene: Lattice Constant versus Interatomic Distance. *Phys. Rev. Lett.* 106:135501-135504.
- Price ML, Ostrovsky D, Jorgensen WL (2001) Gas-Phase and Liquid-State Properties of Esters, Nitriles, and Nitro Compounds with the OPLS-AA Force Field. *J. Comput. Chem.*, 22:1340-1352.
- Ramanathan T, Abdala AA, Stankovich S, Dikin DA, Herrera-Alonso M, Piner RD, Adamson DH, Schniepp HC, Chen X, Ruoff RS et al. (2008) Functionalized Graphene Sheets For Polymer Nanocomposites. *Nat. Nanotechnol.* 3:327-331.
- Rao CNR, Sood AK, Subrahmanyam KS, Govindaraj A (2009) Graphene the New Nanocarbon. *J. Mater. Chem.* 19(17):2457-2469; (2009) Graphene: the new two-dimensional nanomaterial. *Angew. Chem. Int. Ed.* 48(42): 7752-777.
- Rissanou AN, Anastasiadis SH, Bitsanis IA (2009) A Monte Carlo Study of the Coil-to-Globule Transition of Model Polymer Chains Near an Attractive Surface. *J Pol Sci. Part B Pol. Phys.* 47: 2462–2476.
- Rivillon S, Auroy P, Deloche B (2000) Chain Segment Order in Polymer Thin Films on a Nonadsorbing Surface: A NMR Study. *Phys. Rev. Lett.* 84:499-502.

- Stitalsky Z, Tasis D, Papagelis K, Galiotis C (2010) Carbon nanotube-polymer composites: Chemistry, processing, mechanical and electrical properties. *Prog. Pol. Sci.* 35:357-401.
- Steele WA (1973) The Physical Interaction of Gases with Crystalline Solids. *Surf. Sci.* 36:317-352.
- Tatek YB, Tsige M (2011) Structural properties of atactic polystyrene adsorbed onto solid surfaces. *J. Chem. Phys.* 135:174708-1-174708-11.
- Tsoukleri G, Parthenios J, Papagelis K, Jalil R, Ferrari AC, Geim AK, Novoselov KS, Galiotis C (2009) Subjecting a Graphene Monolayer to Tension and Compression. *SMALL* 5:2397-2402.
- Turzi SS (2011) On the Cartesian definition of orientational order parameters. *J. Math. Phys.* 52:053517-1 - 053517-29.
- Williams G, Watts DC (1970) Non-symmetrical Dielectric Relaxation Behaviour Arising from a Simple Empirical Decay Function. *Transactions from the Faraday Society*, 66:80-85.
- Wunderlich W (1989) *Polymer Handbook*, 3rd ed. by J. Brandrup and E.H. Immergut. Wiley: NewYork V 77.
- Yang J-S, Yang C-L, Wang M-S, Chen B-D, Ma X-G (2011) Crystallization of alkane melts induced by carbon nanotubes and graphene nanosheets: a molecular dynamics simulation study. *Phys. Chem. Chem. Phys.* 13:15476-15482.
- Young RJ, Gong L, Kinloch IA, Riaz I, Jalil R, Novoselov KS (2011) Strain Mapping in a Graphene Monolayer Nanocomposite. *ACS Nano* 5:3079-3084.
- Zhao QZ, Nardelli MB, Bernholc J (2002) Ultimate strength of carbon nanotubes: A theoretical study. *Phys. Rev. B* 65:144105-144111.
- Zheng X, Rafailovich MH, Sokolov J, Strzhemechny Y, Schwarz SA, Sauer BB, Rubinstein M (1997) Long-Range Effects on Polymer Diffusion Induced by a Bounding Interface. *Phys. Rev. Lett.* 79:241-244.

Figure Captions

Fig. 1 a Snapshot of a poly(methyl methacrylate) system, which contains 27 polymer chains, confined between two graphene layers. Periodic boundary conditions have been applied on the center of mass of the molecule. **b** A dimmer of a poly(methyl methacrylate) molecule, where the vectors used for the bond order analysis are drawn.

Fig. 2 Monomer density profiles as a function of distance from graphene layers for **a** PMMA1 and PMMA2 systems **b** for PMMA3, PMMA4 and PMMA5 systems. Bulk system's density is represented by a dashed horizontal line in both cases.

Fig. 3 Monomer density profiles as a function of distance from graphene layers based on end (thin lines) and inner monomers (thick lines) of the polymer chain for PMMA5 system.

Fig. 4 Monomer density profiles as a function of distance from graphene layers based on backbone and side groups. Densities are normalized with the corresponding bulk density values. Backbone (thick line), methyl group (thin line) and carboxyl group (dashed line) for **a** PMMA1 and **b** PMMA5 systems.

Fig. 5 Bond order parameter $P_2(\cos\theta)$ along z -axis as a function of distance from graphene layers for two systems. backbone (open squares) and carboxyl group (circles) vectors for **a** PMM3 and **b** PMM5 systems. The corresponding vectors are shown in Fig. 1b. Dashed vertical lines define the boundaries of the adsorption layers.

Fig. 6 Conformation tensor as a function of distance from graphene layers for all PMMA systems. **a** the perpendicular to the surface component, C_{zz} and **b** the average ($C_{//}$) of the two parallel to the surface components C_{xx} and C_{yy} .

Fig. 7 Comparison of the time autocorrelation functions of P_2 among the backbone characteristic vector (solid line), the side group characteristic vector (dashed line) of

PMMA5 and the corresponding bulk vectors, backbone (closed symbols), side group (open symbols). Both characteristic vectors are shown in Fig. 1b.

Fig. 8 The time autocorrelation functions of $R_{ee}(u(t))$ for all PMMA systems.

Fig. 9 The autocorrelation functions of P_2 for the backbone characteristic vector (\mathbf{v}^{bb}) at the different adsorption layers for PMMA5 system. The arrow's direction denotes the increasing distance from graphene.

Fig. 10 a Variation of the segmental relaxation times ($\tau_{\text{segm.}}$) at the different adsorption layers for the backbone (open circles) and the side group (closed stars) characteristic vectors for PMMA5. **b** Variation of the stretching exponents (β) at the different adsorption layers for the backbone (open circles) and the side group (closed stars) characteristic vectors for PMMA5.

Fig. 11 Mean square displacement (MSD) parallel to the surface, based on the monomer centers of mass, as a function of time, at the closest to the graphene adsorption layer (thick line) and the most distant one (thin line) for PMMA5, together with the MSD curve of the bulk system (dashed line).

Fig. 12 Time dependent self diffusion coefficient of the chain centers of mass for PMMA1 and PMMA5 (dashed and solid line respectively) and for the corresponding bulk system (closed symbols).

Table 1

Non-bonded energy parameters for all atom types of PMMA and graphene's carbon (CGR).

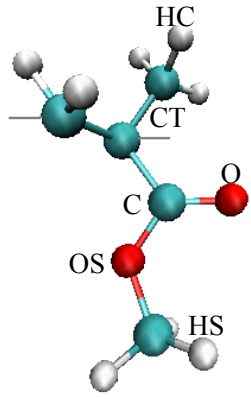
<i>Atom</i>	$\sigma(A)$	$\varepsilon(kJ/mol)$	
HC	0.25	0.1256	
CT	0.35	0.2763	
C	0.375	0.4396	
O	0.296	0.8792	
OS	0.30	0.7117	
HS	0.242	0.0628	
CGR	0.340	0.2327	

Table 2

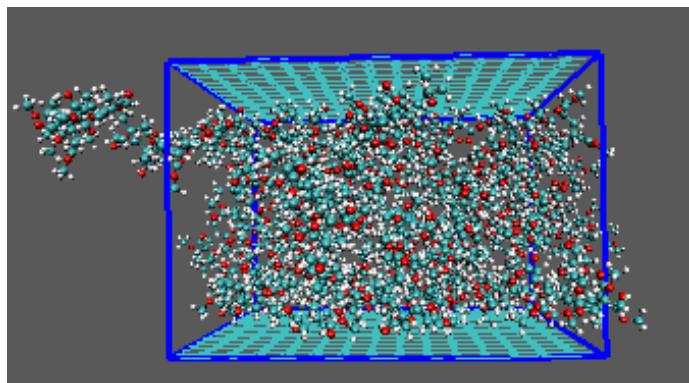
Number of Chains, Film Thickness, Mass fraction of Graphene, Radius of Gyration (R_g) and End-to-End Distance (R_{ee}) for all PMMA systems. Errors are of the order of $0.005nm$ for R_g and $0.05nm$ for R_{ee} .

<i>System</i>	<i>N</i>	<i>d(nm)</i>	<i>Mass fraction of Graphene</i>	<i>R_g(nm)</i>	<i>R_{ee}(nm)</i>
PMMA1	27	2.60	0.372	0.668	1.58
PMMA2	54	5.24	0.229	0.695	1.71
PMMA3	81	7.98	0.165	0.697	1.72
PMMA4	108	10.68	0.129	0.696	1.72
PMMA5	135	13.35	0.106	0.697	1.71
Bulk PMMA	54	-		0.695	1.70

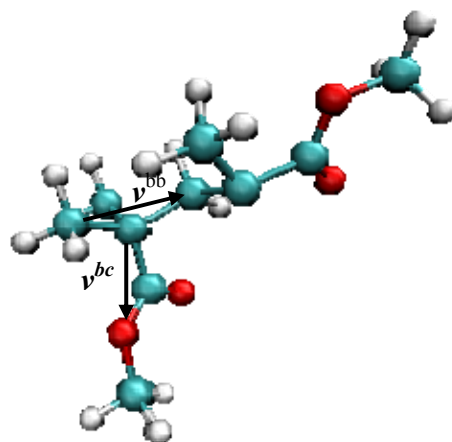
Table 3

Segmental relaxation times (τ_{KWW}) and stretching exponents (β) for v^{bb} , v^{bc} and R_{ee} vectors of all PMMA systems and the corresponding bulk system.

	v^{bb}		v^{bc}		R_{ee}	
	$\tau_{KWW} (ns)$	β	$\tau_{KWW} (ns)$	β	$\tau_{KWW} (ns)$	β
PMMA1	7.0×10^4	0.35	6.0×10^5	0.21	--	--
PMMA2	6.0×10^5	0.38	1.0×10^5	0.31	--	--
PMMA3	1.0×10^5	0.40	2.0×10^4	0.35	--	--
PMMA4	1.0×10^5	0.43	2.0×10^4	0.38	--	--
PMMA5	114	0.43	23	0.41	2.0×10^3	0.65
BULK	37	0.55	9.0	0.49	830	0.61



(a)



(b)

Figure 1

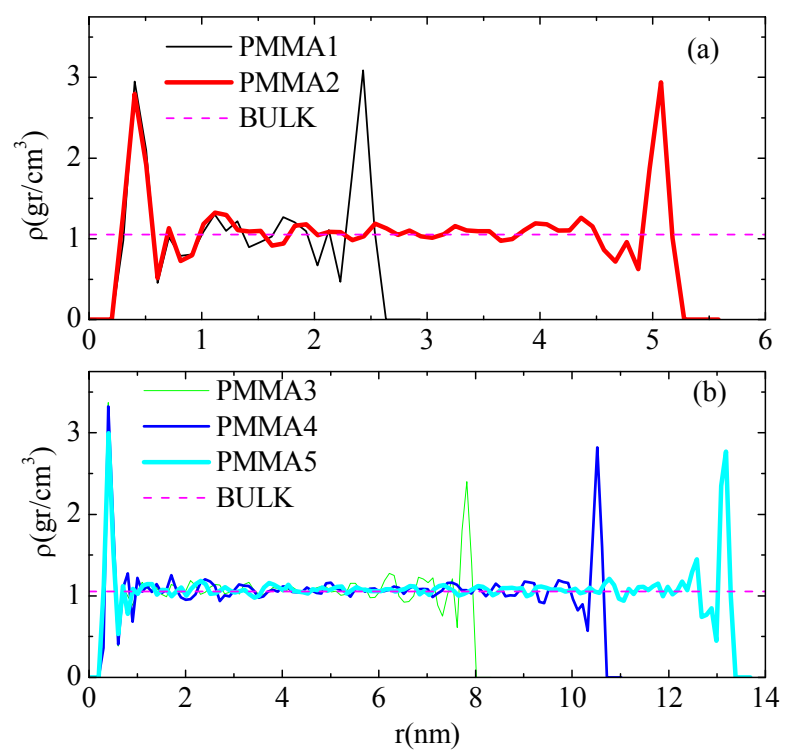


Figure 2

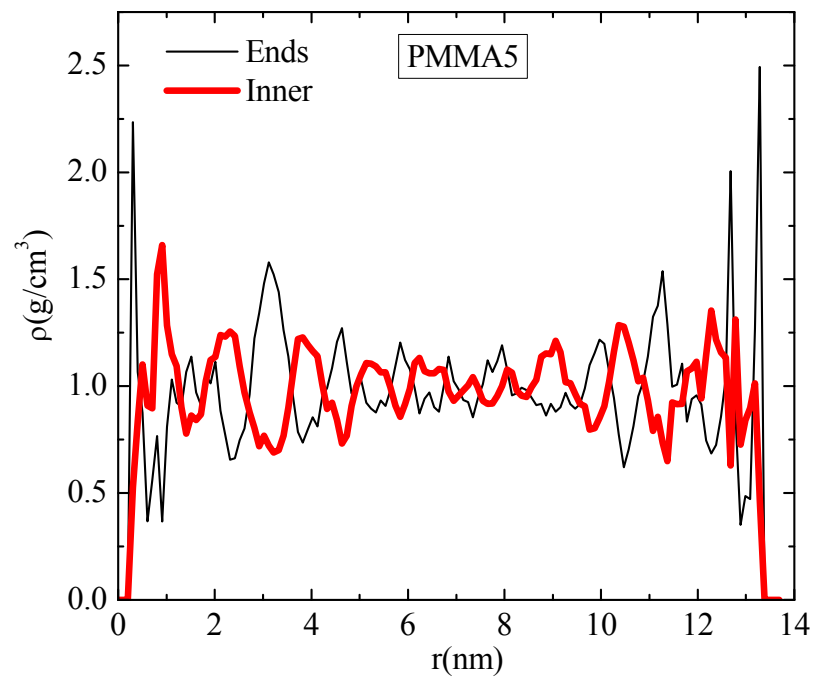


Figure 3

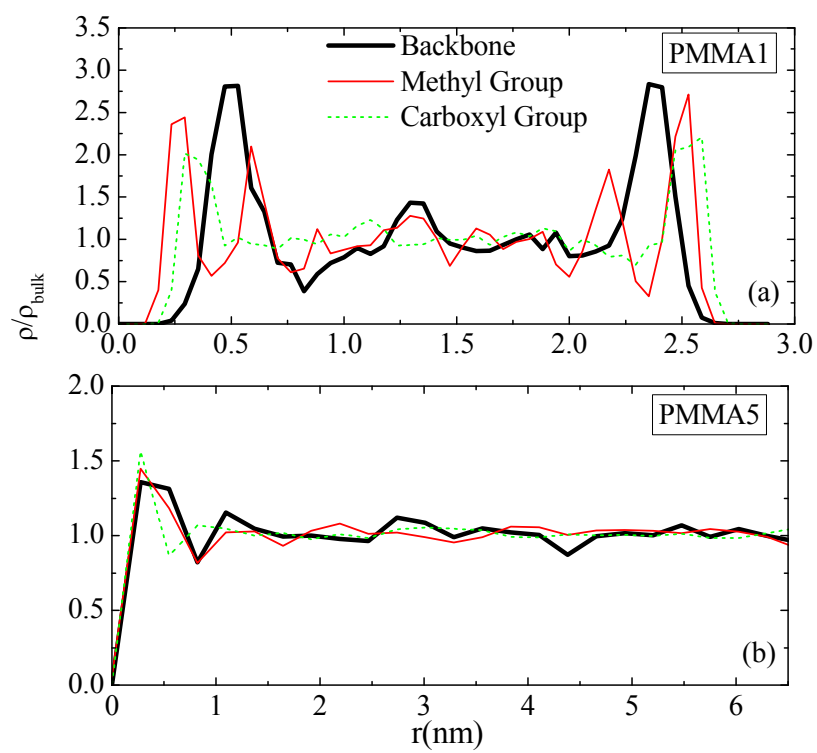


Figure 4

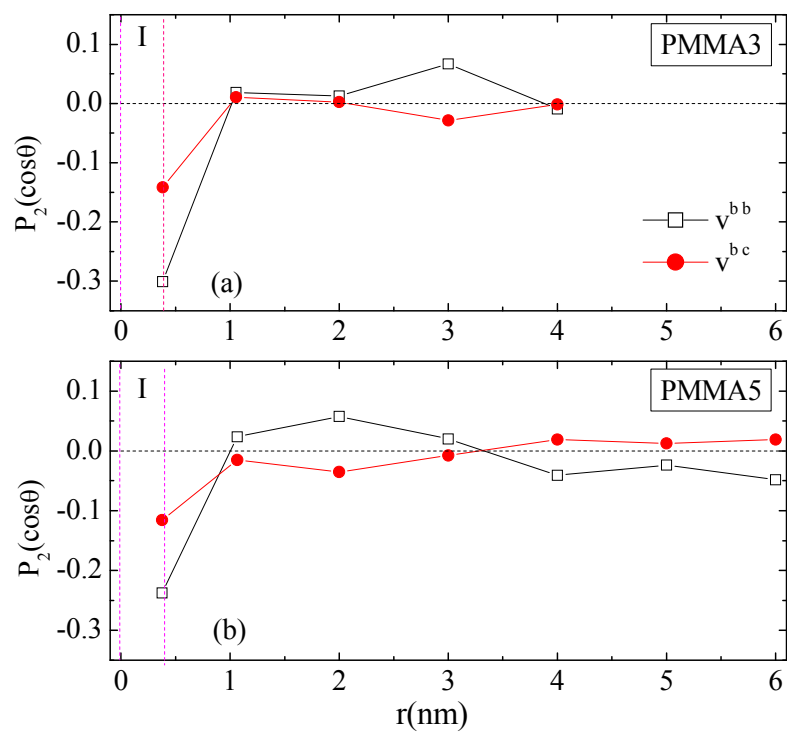


Figure 5

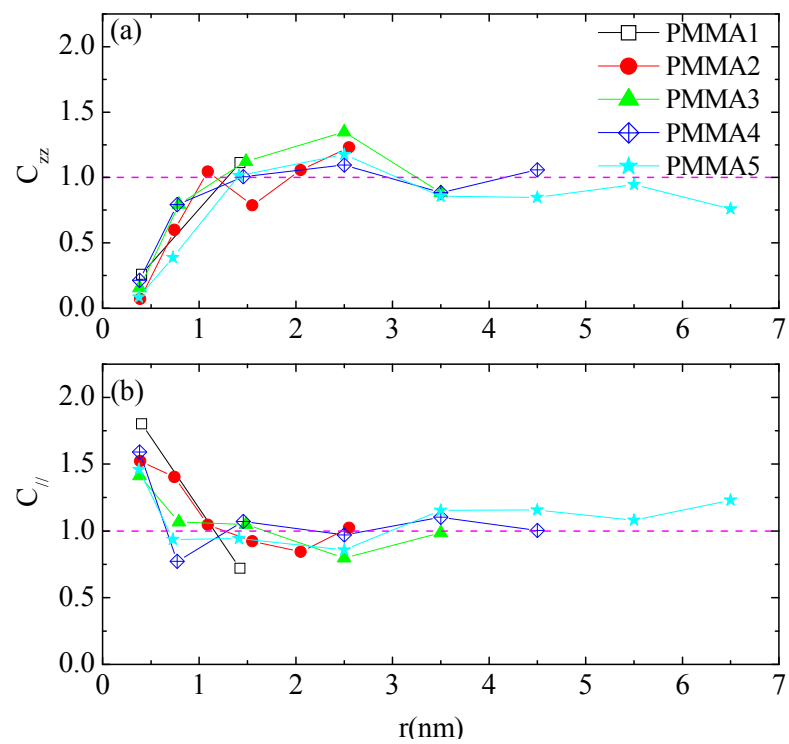


Figure 6

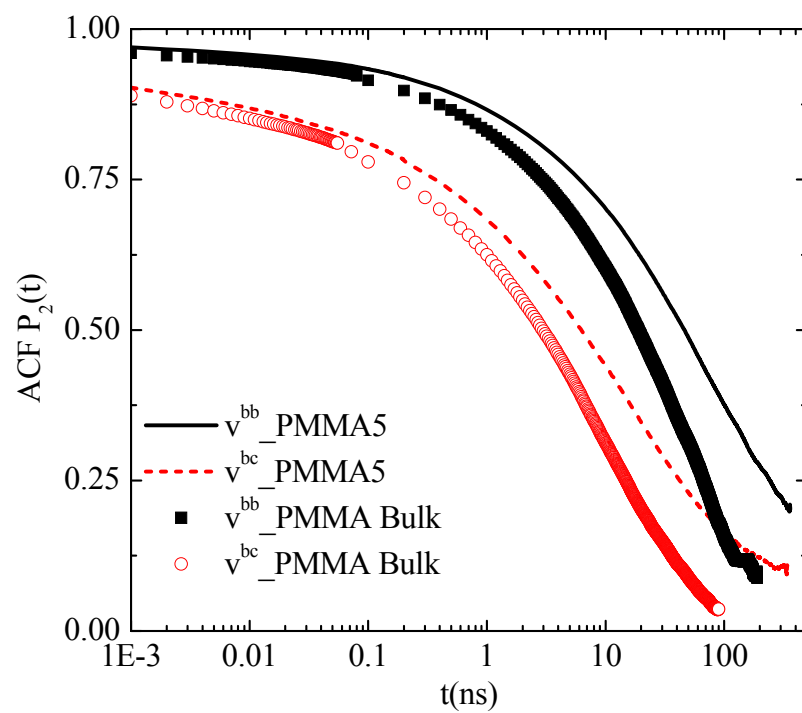


Figure 7

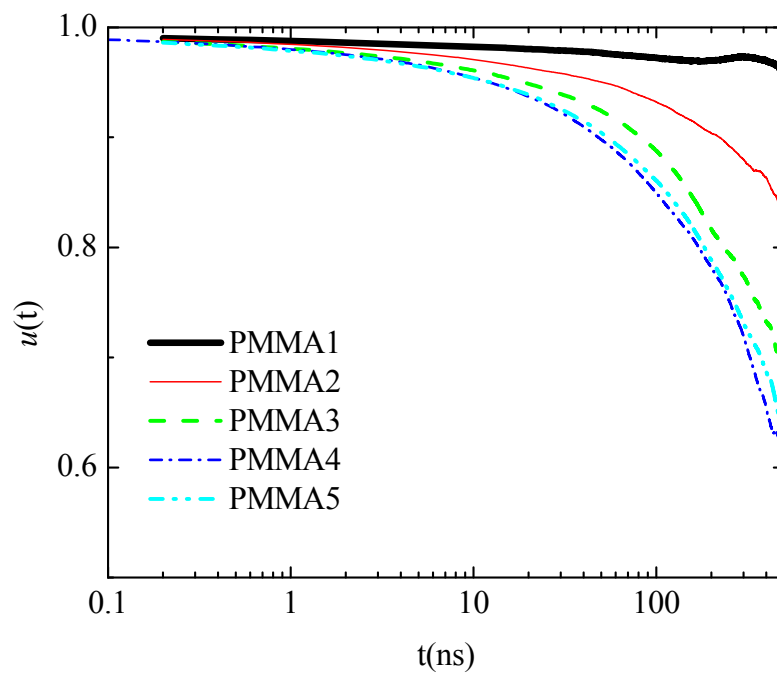


Figure 8

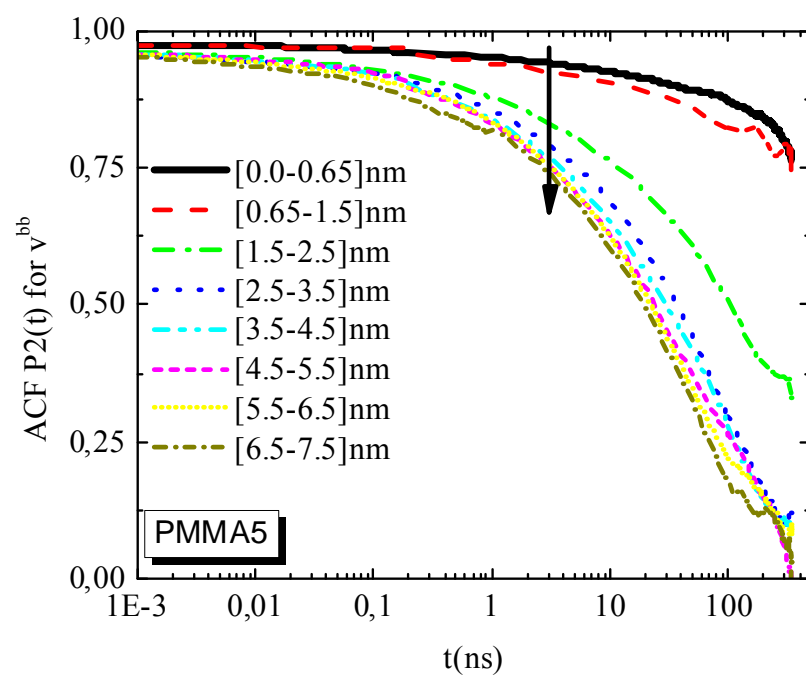


Figure 9

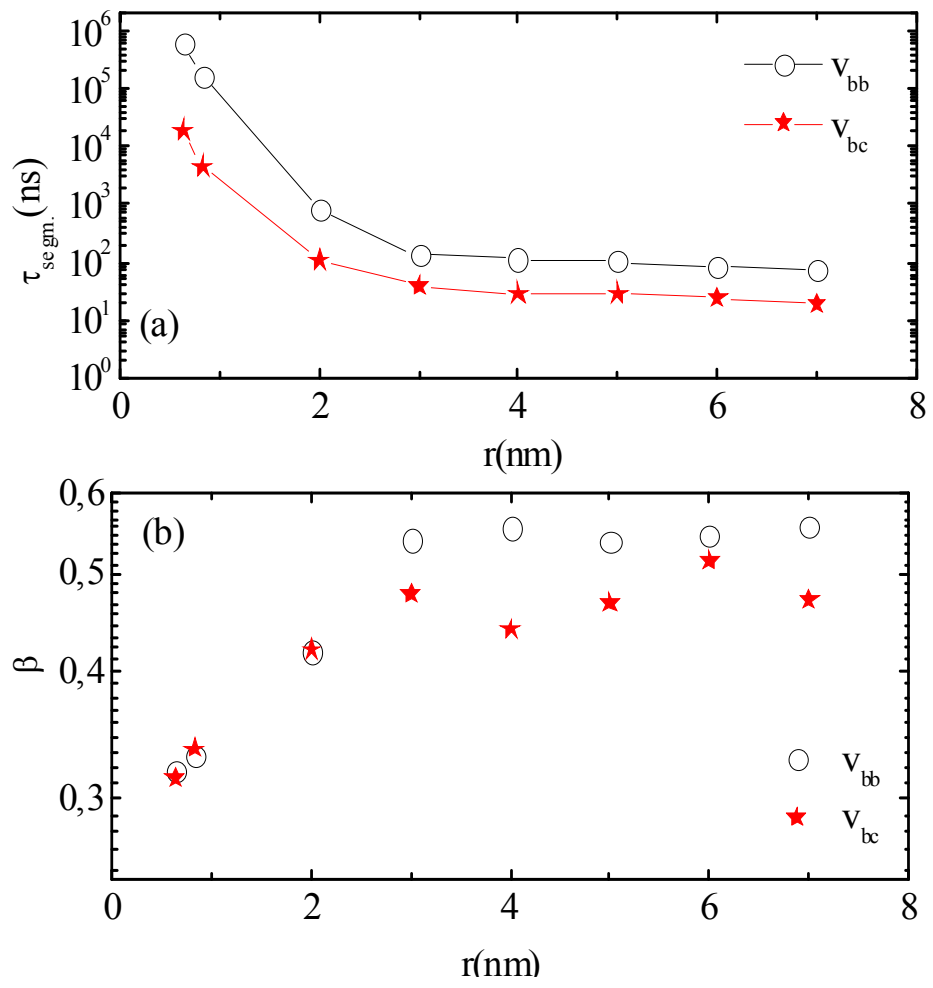


Figure 10

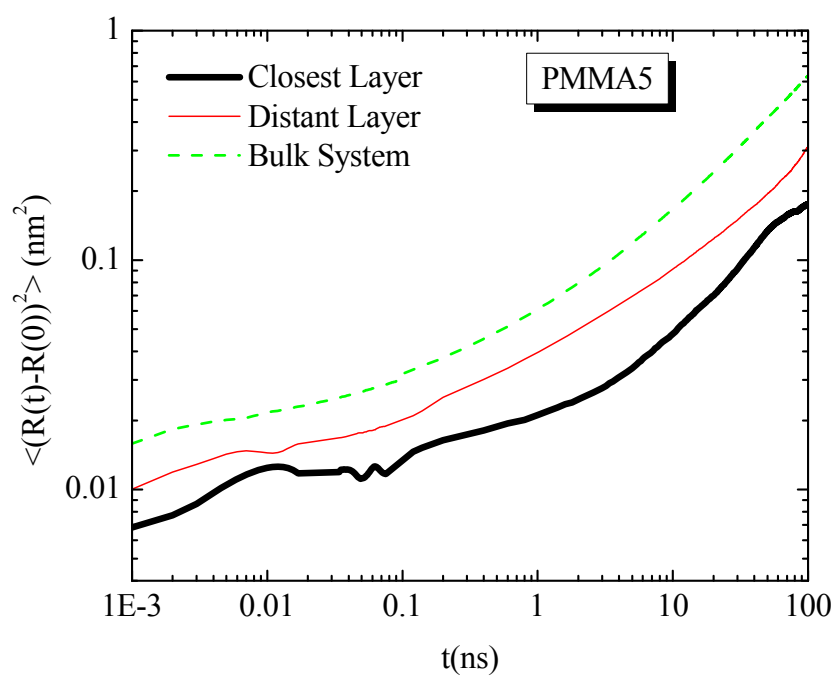


Figure 11

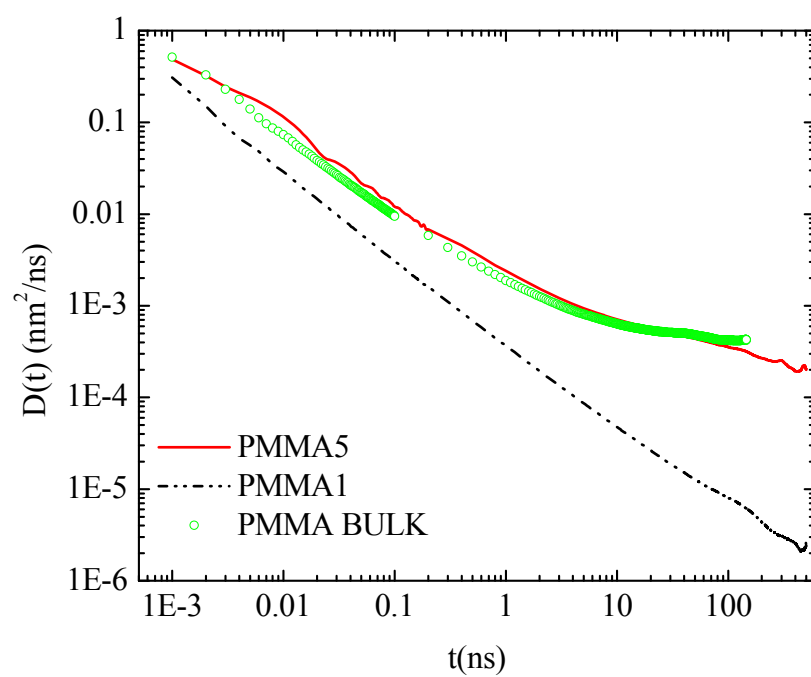


Figure 12